

## Modeling Brain Extracellular Space from Diffusion Data

*Charles Nicholson*

Department of Physiology and Neuroscience, New York University School of Medicine,  
550 First Avenue, New York, NY 10016, USA. [charles.nicholson@nyu.edu](mailto:charles.nicholson@nyu.edu)

### Abstract

The extracellular space (ECS) of the brain is a thin region surrounding each cell that is filled with a medium resembling cerebrospinal fluid and an unknown amount of extracellular matrix. The ECS is difficult to study but diffusion measurements based on a point-source diffusion paradigm have begun to reveal the complex structure of this region. Despite the complexity, a modified version of Fick's classical diffusion equation incorporating parameters for volume fraction and tortuosity has been shown to be valid. Using real-time iontophoresis and the small molecule tetramethylammonium, the volume fraction of typical brain tissue has been determined to be 0.2, i.e. 20% of the brain is ECS and the typical tortuosity is 1.6, which means that a small molecule has an effective diffusion coefficient that is 2.6 less than in free solution. Monte Carlo modeling, however, shows that a simple ensemble of convex cells, each surrounded by a uniform ECS cannot generate a tortuosity greater than 1.225. Further modeling suggests that the discrepancy between experiments and theory may be accounted for by the existence of dead-space microdomains in the ECS; a viscous extracellular matrix might also play a role. Diffusion measurements with integrative optical imaging of fluorescent macromolecules and quantum dots show that tortuosity is increased with macromolecular size and analysis based on the theory of restricted diffusion in pores suggests that the width of the ECS is in the range 38-64 nm.

**Key words:** Brain tissue, extracellular space, volume fraction, tortuosity, dead-space microdomain, extracellular matrix, tetramethylammonium, dextran, quantum dot

### 1. Introduction

The brain enables us to analyze complex scenes and sounds in a fraction of second and is responsible for the performance of exquisite movements orchestrated by a vast array of coordinated muscles. Beyond that, the brain is the source of speech, reasoning, memory and consciousness, but ideas about how this organ works remain very rudimentary. Yet the brain is no more and no less than a vast assemblage of communicating cells. These cells have a complex geometry and are closely packed but they maintain a small space between them, the extracellular space (ECS). This space is vital to brain function and it is equally important as a conduit for the delivery of therapeutic drugs. Unfortunately the ECS is hard to study. By analyzing the diffusion of molecules in the ECS [1, 2] it is possible to build up a picture of the ECS and models are emerging. These models describe different aspects of the experimental data and the challenge for the future is to arrive at a comprehensive description.

## 2. Extracellular space

The ECS has been likened to the “water phase of a foam” [3] with the foam representing the cells. This is a useful but simplistic image. The cells of the brain are actually divided into two types, neurons that communicate by means of electrical and chemical signals and glial cells that are equally numerous but whose overall function remains unclear. Both these types of cell have rounded bodies containing a nucleus but they also have long and often branched extensions that are cylindrical in cross-section for neurons but may be sheet-like for glia. The net effect is a complex ‘neuropil’ (Fig. 1) containing profiles that range in size from less than a micrometer to tens of micrometers. Despite the complexity, the ECS has many of the characteristics of a porous medium and relevant theories from other disciplines can be employed.

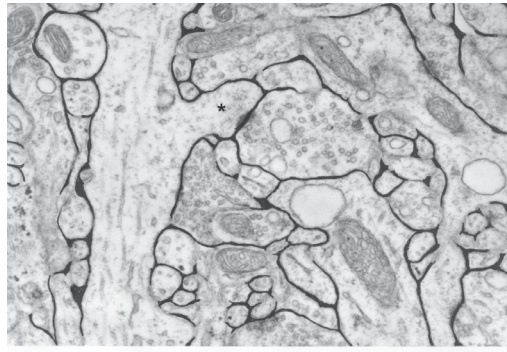


Fig. 1. Electron micrograph of a small region of the cerebral cortex of a rat. The black areas between cells indicate the ECS, which probably has been reduced in width during histological processing. Scale bar represents about 1  $\mu\text{m}$ . Reproduced from [1].

In Fig. 1 the ECS has been filled in (black lines) and it is evident that every cell membrane is surrounded by a thin ‘atmosphere’ of ECS. This atmosphere contains a fluid that is similar in composition to the cerebrospinal fluid that baths the outer surface of the brain and is present in large internal cavities or ventricles and in the spinal canal. This fluid is predominantly composed of sodium and chloride dissolved in water with much smaller amounts of other substances, including potassium and calcium. There is another entity in the ECS and that is the extracellular matrix. This matrix is composed of long-chain molecules that have many negative charges. Among the main components are hyaluronan and chondroitin sulfate [4]. One problem is that it is not known how much matrix is present in the ECS and it probably varies with different brain region. If there is a lot of matrix then it will increase the viscosity experienced by a diffusing molecule.

## 3. Diffusion concepts applied to the ECS

Because the ECS is essentially a fluid-filled space it does not survive well the tissue processing that is required to produce an electron micrograph and typically the width of the space is reduced. But beyond that, the dynamic properties of the ECS – how it influences molecular transport for example – cannot easily be estimated from 2D fixed sections of the brain. This type of information can be revealed from diffusion measurements.

Early work on diffusion in the brain used radiotracers, such as sucrose, that could be expected to remain largely confined to the ECS. Typically, one surface of the brain was bathed in the tracer for some time, allowing the substance to penetrate and form a concentration gradient. Then the tissue was fixed and cut as a sequence of small blocks perpendicular to the surface, the tracer in each was quantified and the diffusion properties of the brain region estimated [1, 5].

More recent diffusion measurements have used variations of a ‘point-source paradigm’, largely developed in our laboratory, to reveal the ‘real-time’ diffusion properties of small regions of brain tissue (Fig. 2). The crux of this method is to use a glass micropipette with a tip diameter of only a few micrometers to release a small quantity of a substance into the ECS and then monitor the subsequent concentration of the substance as a function of time and position. This paper will be based primarily on data obtained with such a paradigm, but the results are in agreement with the radiotracer studies.

The fundamental hypothesis behind all these measurements is that small substances that enter the ECS and remain confined to this domain will move predominantly by diffusion. Because diffusion is a macroscopic expression of an ensemble of microscopic random walks, molecules will explore the structure of the ECS and the concentration distribution will reveal important parameters of the local structure [2]. The most important parameters are volume fraction and tortuosity.

For an ideal molecule, i.e. one that stays in the ECS, volume fraction ( $\alpha$ ) is defined as

$$\alpha = V_{\text{ECS}}/V_{\text{Tissue}} \quad (1)$$

where  $V_{\text{ECS}}$  is the volume of the ECS and  $V_{\text{Tissue}}$  is the volume of the entire tissue. Both volumes are defined with respect to some Representative Elementary Volume (REV), typically for the point-source paradigm of the order of  $10^6 \mu\text{m}^3$ . If electron micrographs were perfect,  $\alpha$  could be obtained from stereological measurements on images, such as that shown in Fig. 1, by simply comparing surface areas or line segments.

Tortuosity ( $\lambda$ ) is a more complex parameter than volume fraction but it is easy to define operationally as

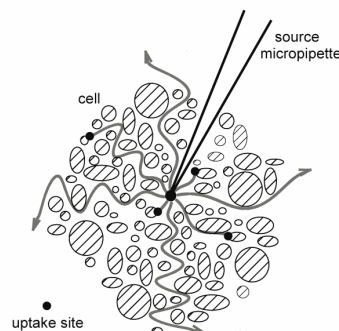


Fig. 2. Point-source paradigm for diffusion studies. Glass source micropipette is filled with small probe molecules that are released into the ECS. The micropipette tip is a good approximation of a point source. Released molecules diffuse (lines with arrowheads) through the ECS around cellular elements. Some molecules may be removed from the ECS at uptake or loss sites (*black dots*).

$$\lambda = \sqrt{D/D^*} \quad (2)$$

where  $D$  is the diffusion coefficient for the ideal molecule measured in a free solution, often a very dilute agarose gel (0.3% w/v) made up with a salt solution that mimics the major components of the fluid in the ECS, and  $D^*$  is the effective diffusion coefficient measured in the brain (note that in chemical engineering the tortuosity is generally equated to  $D/D^*$  rather than  $\sqrt{D/D^*}$ ).

The governing diffusion equation linking  $\alpha$  and  $\lambda$  is then defined as a modification of Fick's second law

$$\frac{\partial C}{\partial t} = \frac{D}{\lambda^2} \nabla^2 C + \frac{Q}{\alpha} - F_{\text{Loss}}(C) \quad (3)$$

where  $Q$  is a source term and  $F_{\text{Loss}}(C)$  is a term that accounts for any loss of molecules from the ECS. For ideal molecules, loss will be zero. There are several important caveats regarding this equation. The first is that the concentration measured along any line in the tissue is actually discontinuous because the intracellular concentration is zero for an ideal molecule so that the rigorous derivation of the diffusion equation involves a volume-averaging process over the appropriate REV [1, 6]. This process also provides a justification for the tortuosity. The second caveat is that in Eq. (3), and throughout this paper, the concentration  $C$  is defined as the actual concentration measured in the ECS. This is the physiologically relevant variable because it is what a receptor on a cell membrane experiences and that is also the concentration measured in most experiments described here. However, other disciplines and some experiments use concentration per unit volume of tissue,  $C_1$ . It is clear that  $C_1 = \alpha C$  but failure to recognize which definition is in use can result in a misinterpretation of the literature. The third caveat is that bulk flow within the ECS has been neglected because it is negligible in the experiments that form the basis of this paper. Bulk flow refers to hydrodynamic flow within the ECS, which is probably confined to a narrow perivascular space around some blood vessels in normal tissue (see [1] for more detail).

Because  $D^* < D$  it follows that  $\lambda > 1$  and consequently tortuosity may be thought of as a measure of the hindrance that the brain places on a diffusing molecule with respect to a free medium. As will become apparent, however, the interpretation of  $\lambda$  in terms of specific structure is an entirely separate process from its definition given by Eq. (2), so tortuosity is not as conceptually simple as volume fraction.

#### 4. Measurements with small ‘ideal’ molecules

The first realization of the point-source paradigm considered here is the real-time iontophoresis method using tetramethylammonium, abbreviated as the RTI-TMA method. TMA<sup>+</sup> is a small cation of 74 molecular weight that approximates an ideal point molecule that may be expected to explore the entire ECS. The concentration of TMA<sup>+</sup> as a function of time  $t$  at a distance  $r$  from the

point source micropipette can be sensed with an appropriate ion-selective microelectrode (ISM). A typical experimental arrangement is shown in Fig. 3. The appropriate solution to Eq. (3), described in [1, 6], is

$$C(t) = \frac{Q}{8\pi D^* \alpha r} \left[ \operatorname{erfc}\left(\frac{r}{2\sqrt{D^*t}} + \sqrt{k't}\right) \exp\left(r\sqrt{\frac{k'}{D^*}}\right) + \operatorname{erfc}\left(\frac{r}{2\sqrt{D^*t}} - \sqrt{k't}\right) \exp\left(-r\sqrt{\frac{k'}{D^*}}\right) \right]. \quad (4)$$

Some TMA<sup>+</sup> is lost from the ECS, either into cells or across the blood-brain-barrier and this is accounted for by setting  $F_{\text{Loss}}(C) = k'C$  in Eq. (3). Eq. (4) assumes that the source  $Q$ , which is a point-source in space, is begun at time  $t = 0$  and continues to infinity. To obtain the solution for a finite pulse of duration  $t_p$ , a delayed form of Eq. (4) must be subtracted from the infinite duration solution

$$C = C(t) - C(t - t_p), \quad t > t_p. \quad (5)$$

Finally,  $Q$  itself is defined in terms of the applied iontophoretic current  $I$  and transport number of the source electrode  $n_t$  as  $Q = I n_t / zF$  where  $z$  is the valency of the ion (+1 for TMA<sup>+</sup>) and  $F$  is Faraday's Electrochemical Equivalent. For a detailed description of the method see [6 – 8].

Non-linear curve fitting of Eqs. (4) and (5) to experimental data obtained in a dilute agarose gel (where  $\lambda = 1$ ,  $\alpha = 1$ ,  $k' = 0$ ) determine  $D$  and  $n_t$  and then similar curve fitting in brain tissue provides  $D^*$  and  $\alpha$ . From  $D$  and  $D^*$  the tortuosity is calculated using Eq. (2). The value of  $k'$  is also obtained in brain tissue but this is really a correction factor for the non-ideal behavior of TMA<sup>+</sup> and not a fundamental parameter so it will not be

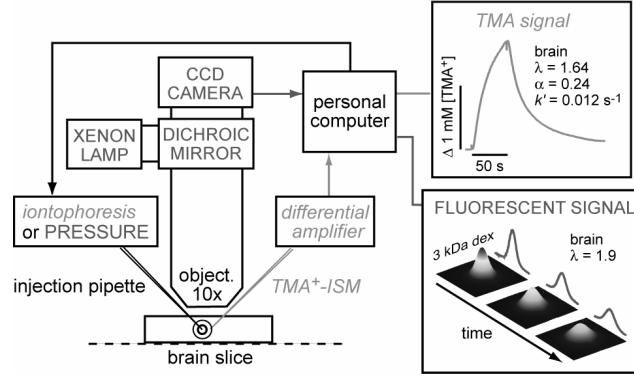


Fig. 3. Recording setup for diffusion measurements using real-time iontophoretic (RTI) and integrative optical imaging (IOI) methods. See text for details.

considered further here. The data acquisition and analysis are performed by custom software (Wanda and Walter, available from C. Nicholson).

## 5. Data and models for small ‘ideal’ molecules

From more than 30 peer-reviewed studies with the RTI-TMA method carried out predominantly in our laboratory in New York and the laboratory of Prof. Eva Syková in Prague it can be said that the diffusion equation (Eq. 3) is applicable to brain tissue. Further, it is established that in normal brain tissue  $\alpha = 0.2$ , i.e. 20% of the brain is actually ECS, and  $\lambda = 1.6$ , i.e. a small molecule has an effective diffusion coefficient that is reduced by about

2.6 compared to that in a free medium. Of course there are deviations from these values in some regions of the brain, for example diffusion is anisotropic in the cerebellar molecular layer [9] and in fiber tracts of the brain such as the corpus callosum [10] but on the whole the similarities in results are more striking than the differences and the same values occur in a range of species.

### 5.1 Equally-spaced convex cell models

Can a model account for  $\alpha = 0.2$  and  $\lambda = 1.6$ ? The most elementary model is to return to the idea of the ECS as the water phase of a foam but to simplify the problem even further by representing the cells by cubes of uniform size and equal spacing (Fig. 4A). By choosing an appropriate cube size and spacing,  $\alpha$  will be specified and then  $\lambda$  can be estimated by running a Monte Carlo simulation. For the simulation, a large number of point particles are released from a point source in the middle of an ensemble of many cubes and the particle distribution after a certain number of time steps is measured. It is assumed that each particle moves within the ECS with a diffusion coefficient  $D$  while making occasional specular collisions with the walls of the cubes. Because cubes are space-filling, the value of  $\alpha$  can be varied from 0 to a value approaching 1 (free medium without cells) and a range of  $\lambda$  is obtained. This plan was implemented by Tao & Nicholson [11] using the program MCell developed for simulating some other neurobiological problems [12]. The simulations suggested that a simple relation

$$\lambda = \sqrt{(3 - \alpha)/2} \quad (6)$$

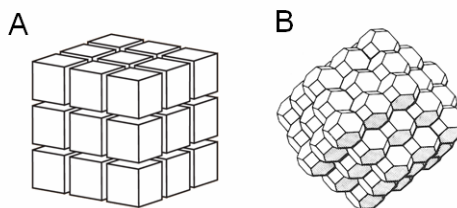


Fig. 4. Simple models of ECS. A. Ensemble of cubes. B. Ensemble of truncated octahedra.

exists between  $\alpha$  and  $\lambda$ . Remarkably, this is the same result that was obtained by James Clerk Maxwell in 1891 (See [13]) for a dilute suspension of spheres. Some work has indicated that Maxwell’s result should hold for more densely packed structures [14]. The maximum value of  $\lambda$  occurs in Eq. (6) when  $\alpha \rightarrow 0$  (this is possible because a point particle of negligible size is being used) and in this limit  $\lambda \rightarrow \sqrt{3/2} = 1.225$ . This limiting value was also derived by other investigators using different approaches (e.g. [15 – 17]).

Cubes pack with long aligned channels (Fig. 4A) however, so to confirm that Eq. (6) and its limiting value were not related to this feature, Tao and Nicholson [11] used two other space-filling sets of objects, namely truncated octahedra (Fig. 4B) and a combination of rhombicuboctahedra, cubes and tetrahedra. The results were exactly the same as for cubes and it was hypothesized that the result held for any set of space-filling convex cells that had uniform spacing. A more sophisticated Monte Carlo simulation with pseudo-random shapes further confirmed this [17].

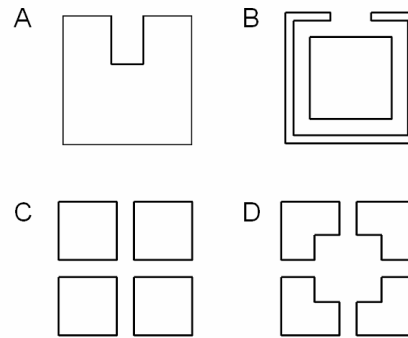


Fig. 5. Dead-space microdomains. A. 2D representation of a cubic cell with a cavity or ‘pocket’ dead-space. B. Cubic cell partially wrapped by a sheet-like glial cell. The wrapping forms a dead-space. C. Four cubic cells with uniform spacing (no dead-space). D. Four cubic cells deformed to allow a void dead-space to form at center.

## 5.2 Dead-space microdomain models

The equally-spaced convex cell results raise an important problem when compared with the experimental data showing that usually  $\lambda = 1.6$  with  $\alpha = 0.2$  because the models described by Eq. (6) give  $\lambda = 1.183$  for  $\alpha = 0.2$  and the maximum value cannot exceed 1.225. This prompted an examination of the underlying assumptions of the model. The first assumption was that the cells had to be convex. As noted in Section 2, the cells of the brain have a very complex geometry; in 2D sections the majority of profiles can appear convex but may actually be different in 3D. This leads to the hypothesis that concave elements might exist, either as invaginations of a cell membrane (Fig. 5A) or as a more extensive enveloping sheet-like configuration (Fig. 5B). Both these cases amount to dead-space microdomains that are not well-connected with the rest of the ECS. By this it is meant that a diffusing particle upon entering such a microdomain explores it for a while and then exits at the same location that the particle entered. Thus the particle does not advance towards its goal but merely loses time. For suitable geometries and diffusion processes this is known to increase the effective diffusion coefficient (e.g. [18]).

Hrabětová and co-workers [19] have provided experimental evidence for the existence of dead-space microdomains in ischemic brain tissue and it is plausible, but not completely established, that such dead-spaces might exist in normal tissue. A model based on dwell-times was proposed [19] and more rigorously analyzed by Hrabe et al. [17] that yields, for small microdomains and volume fractions in the range encountered in brain tissue, the basic formula

$$\lambda = \lambda_0 \sqrt{\alpha / (\alpha - \alpha_d)} \quad (7)$$

where  $\lambda_0 = 1.225$  is the limiting volume fraction derived from Eq. (6),  $\alpha_d$  is the volume of the dead-space microdomains and  $\alpha$  is the total volume fraction of the ECS. The well-connected extracellular space with volume fraction  $\alpha_0$ , is that remaining after elimination of the dead-spaces so  $\alpha = \alpha_0 + \alpha_d$ . Application of Eq. (7) to experimental results has revealed that the ratio  $\alpha_d : \alpha_0$  would be expected to be about 40:60 in normal cortical tissue and 60:40 in pathological ischemic tissue ([19, 20]).

These results were generalized to larger microdomains and volume fractions [21], based on detailed Monte Carlo simulations, resulting in the expression

$$\lambda = \sqrt{\left(\frac{3-\alpha}{2}\right) \left(\frac{\alpha}{\alpha - \alpha_d}\right)^{1/\beta}} \quad (8)$$

where  $\beta$  is an empirical parameter in the range 2 – 3. These simulations also covered the case where the dead-space took the form of a local enlargement of the ECS or a local void (Fig. 5C, D). These voids also delay particles because, once they enter such a region they take some time to find their way out again. This result is known in 2D [22, 23]. The void result deals with the second assumption that was made in the simple model, namely that the spacing between cells remained constant. Introducing local enlargements violates this condition and increases  $\lambda$ .

The two cavity models (Eq. 7 and Eq. 8) are plotted in Fig. 6 for fixed values of  $\alpha_d$  along with the cavity-free Eq. (6). For Eq. (8),  $\beta = 2$  corresponds to a ‘pocket’ (Fig. 5A) while  $\beta = 3$  is appropriate for a void (Fig. 5C,D); see [21] for more detail. It is evident that the presence of cavities dramatically increases  $\lambda$  as  $\alpha$  diminishes.

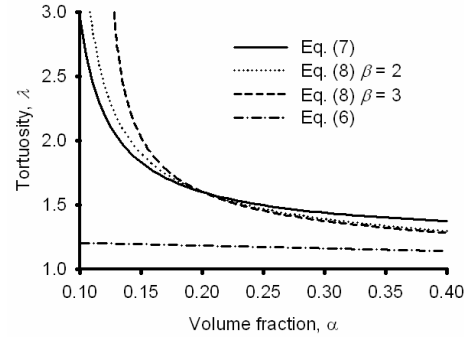


Fig. 6. Tortuosity as a function of  $\alpha$  for a fixed  $\alpha_d$ . For Eq. (7)  $\alpha_d = 0.083$ ; for Eq. (8),  $\beta = 2$ ,  $\alpha_d = 0.091$ , and  $\beta = 3$ ,  $\alpha_d = 0.119$ . These values ensure that when  $\alpha = 0.2$ ,  $\lambda = 1.6$ . Eq. (6), the case with no cavities, is plotted for comparison.

It is worth noting that the limiting value of  $\lambda$  for 2D ensembles of squares or other convex structures is  $\sqrt{2} = 1.414$  [15], which is greater than the value of 1.225 that applies to 3D convex cells. Furthermore, if the ECS is composed of connected tubes instead of the planes that underlie Eq. (6), the limiting value of  $\lambda$  is  $\sqrt{3} = 1.732$  [15]. Thus the tortuosity is a subtle measure of connectivity and geometry and this makes it difficult to estimate it from simple models because they often fail to take into account all the possible pathways, or local delays, inherent in the geometry [17, 23]. Indeed, Torquato [24] has argued that the sort of random media under discussion here require an infinite set of  $n$ -point correlation functions in order to characterize them completely.

### 5.3 Extracellular matrix models

The previous arguments show that the basic geometrical tortuosity associated with an ensemble of uniformly spaced convex cells can be increased by introducing a more complex geometry and this strategy will be capable of elevating the value of  $\lambda$  to 1.6 or more for a volume fraction of 20%. This is not, however, the only way in which tortuosity might be increased; the extracellular matrix could also accomplish this. If the matrix is regarded as a polymer solution then a large literature may be applied to its representation [25, 26]. An attempt to model both the geometrical and viscous components of tortuosity in brain tissue was made by Rusakov & Kullmann [27]. But because so little is known about the extent of the matrix, such elaboration may be unwarranted and simpler models suffice that just represent the viscosity of the ECS as greater than that of a free solution. Because  $\lambda$  can always be formally decomposed into a set of multiplicative components

$$\lambda = \sqrt{\frac{D}{D^*}} = \sqrt{\frac{D_1}{D^*} \frac{D_2}{D_1} \cdots \frac{D_n}{D_{n-1}} \frac{D}{D_n}} \quad (9)$$

it is plausible that  $\lambda$  can be expressed as the product of a geometrical tortuosity described above and a viscous component i.e.  $\lambda = \lambda_{\text{geom}} \lambda_{\text{visc}}$ . It has also been suggested from physiological experiments that the introduction of 5% 40 kDa dextran into the ECS increases ECS viscosity [28] so an intrinsic matrix might have a similar effect.

### 6. Measurements with macromolecules

While  $\text{TMA}^+$  and some other small ions have been excellent probes of the ECS they do not tell us how a much larger molecule would behave. Many important signaling agents in the brain are macromolecules (e.g. nerve growth factors). Furthermore, the diffusion of large molecules can reveal new properties of the ECS; the latter perspective is emphasized here.

The RTI method used with  $\text{TMA}^+$  cannot be applied to macromolecules both because it is usually difficult to iontophorese large molecules and because it is not possible to fabricate ISMs that can sense macromolecules. To study macromolecules, Nicholson and Tao [29] introduced a variant of the point-source paradigm which they called Integrative Optical Imaging (IOI).

In the IOI method (Fig.3), macromolecules carrying a fluorescent label are released from a micropipette by a short pressure pulse and the resulting diffusing cloud of molecules imaged using a conventional epifluorescent microscope equipped with a digital camera connected to a PC [29, 30]. If the pulse is very brief compared to the duration of subsequent diffusion processes, then it can be regarded as a delta function in both time and space and the appropriate solution (see [1, 29]) to Eq. (3) is:

$$C(r, t_i) = \frac{UC_f}{\alpha} \frac{1}{(4D^*(t_i + t_0)\pi)^{3/2}} \exp\left(-\frac{r^2}{4D^*(t_i + t_0)}\right), \quad (10)$$

where a volume  $U$ , of the macromolecular solution at concentration  $C_f$  is ejected. The variable  $t_0$  represents a virtual source time origin such that the source appears to have been activated at time  $t_0$  before it actually occurred. This allows a point-source formalism to be employed even when a finite initial volume is released (see [31]). Because large molecules do not easily leave the ECS, no loss term is needed, i.e.  $F_{\text{Loss}} = 0$  in Eq. (3).

To make use of Eq. (10) it is necessary to relate the image intensity distribution recorded by the camera to the concentration. The theory of how the image of the diffusing cloud of molecules maps onto the plane of the camera is complicated [29, 32] but it may be shown that Eq. (10) can be reduced to Eq. (11). In both Eq. (10) and Eq. (11) a discrete time  $t_i$  is used to represent the sequence of camera images:

$$I_i(r, \gamma_i) = E_i(\gamma_i) e^{-\gamma_i^2 / r_i^2} \quad \text{and} \quad \gamma_i^2 = 4D^*(t_i + t_0) \quad (11)$$

where  $I_i$  is the intensity of the fluorescence and  $E_i$  is an amplitude term embodying the defocussed point-spread function of the objective [29, 32]. By fitting the exponential term in Eq. (11) to the spatial distribution at a sequence of times  $t_i$ ,  $D^*$  can be determined [29]. Control diffusion measurements to determine  $D$  are made in dilute agarose and then  $\lambda$  is calculated from Eq. (2). The actual data analysis is carried out using custom software (Vida and Ida, available from C. Nicholson and described in more detail in [30]).

## 7. Data and models for macromolecules

The diffusion of a variety of globular and flexible chain molecules in brain tissue has been reported in several papers. Here attention will be confined to molecules with a globular structure where a meaningful hydrodynamic diameter can be estimated from the free diffusion coefficient using the Stokes-Einstein equation [33]

$$d_H = \frac{k_B T}{3\pi\eta D} \times 10^{13} \quad (12)$$

where  $d_H$  is the molecule diameter (nm),  $k_B$  is Boltzmann's constant ( $1.38065 \times 10^{-23}$  J.K<sup>-1</sup>),  $T$  is temperature (K),  $\eta$  is viscosity (Pa.s) in the solvent (usually water) and  $D$  is the free diffusion coefficient (cm<sup>2</sup> s<sup>-1</sup>).

Two types of globular macromolecules may be considered: dextrans and proteins. Dextrans are aggregates of long-chain sugar molecules that form a loose ball in solution and only have an approximate molecular weight. In contrast, proteins are rigid molecules with a well defined structure, parts of which may make specific interactions with receptors on cells or components of the extracellular matrix. For the protein studies referenced here, such specific interactions are either non-existent or have been suppressed, so both types of molecule probe the more general properties of the ECS.

Using dextrans ranging from 3 kDa to 70 kDa and proteins ranging from 6.6 kDa to 66 kDa in slices of rat brain it is a general finding that the measured tortuosity is no longer 1.6 but ranges from about 1.7 – 2.5 and there is a steady increase in  $\lambda$  with molecular weight (Fig. 7). Thus larger molecules are more hindered, probably through increasing interaction with the membranes that define the ECS.

### 7.1 Models to estimate the width of the ECS

The increase in tortuosity with molecular size prompts the question of what is the largest molecule that can diffuse through the ECS. In principle one could answer this by selecting a range of molecules of ever increasing size until one was reached that no longer diffused. In practice, however, this is not possible because the time needed to determine the effective diffusion coefficient in the tissue would eventually exceed the viable lifetime of the biological preparation, as the chosen molecules diffused ever more slowly. To make practical measurements, Thorne and Nicholson [38] turned to the theory of restricted diffusion (RD) in narrow pores and probed the diffusion properties of the anesthetized *in vivo* rat cortex with a recently developed nano-particle, the quantum dot.

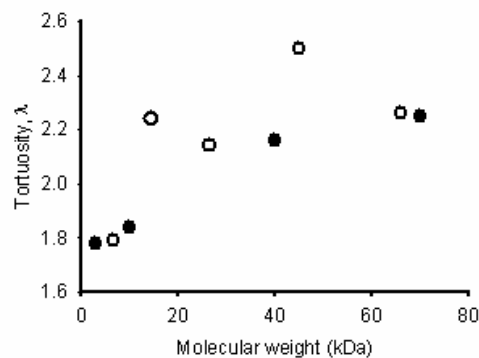


Fig. 7. Tortuosity versus molecular weight for macromolecules in rat brain slices. Filled circles are dextrans and open circles are proteins. Data based on [29, 31, 34 –37].

Quantum dots (QDs) are nanocrystals that have a core which emits fluorescent light at a precise frequency. The core is enclosed in a protective shell and, for use in the diffusion studies, the shell must be coated with short strands of polyethylene glycol (PEG) to make the QD water soluble and inert. A QD with a final diameter of 35 nm (QD655, manufactured by Invitrogen, Carlsbad, California, USA) was chosen and diffusion measurements were made with the IOI technique along with measurements of 3 and 70 kDa dextrans. The QD did diffuse but with  $\lambda = 10.6$ , a value of unprecedented magnitude.

To interpret these results in terms of the width of a channel required to allow a QD to diffuse, a similar decomposition of the tortuosity to that described for the matrix (Eq. 9) may be used

$$\lambda = \sqrt{\frac{D}{D^*}} = \sqrt{\frac{D'}{D^*} \frac{D}{D'}} \cong \lambda_{\theta=0} \sqrt{\frac{D}{D'}} \quad (13)$$

where  $D'$  is the interstitial diffusion coefficient. For neutral, inert substances subject to purely steric interactions with pore walls,  $D'/D$  only depends on channel geometry and  $\theta$ , the ratio of probe hydrodynamic diameter,  $d_H$  (Eq. 12) to brain ECS width,  $d_{ECS}$ , i.e.  $\theta = d_H/d_{ECS}$ . The parameter  $\lambda_{\theta=0}$  is the tortuosity for a vanishingly small molecule.

Broadly speaking there are two types of RD model that might apply to the ECS, a plane model or a cylinder model (Fig. 8). The previous discussion makes it plausible that the ECS is a set of intersecting planes and therefore the theory developed by Deen, [39] would be appropriate. However the actual space in which a large molecule moves might be reduced to a set of interconnected tubes or cylinders because of the presence of the matrix. To a macromolecule the ECS might appear as a set of connected tunnels through the matrix, then the theory of Bungay & Brenner, [40] would be appropriate. In either case, appropriate expressions for  $D'/D$  can be inserted into equation (13) resulting in two free parameters,  $d_{ECS}$  and  $\lambda_{\theta=0}$ . Taking the example of parallel plane geometry [39]:



Fig. 8. Pore models. A. Molecule (filled circle, diameter  $d_H$ ) in planar pore (diameter  $d_{ECS}$ ). B. Molecule in cylindrical pore.

$$\sqrt{\frac{D}{D'}} = \left[ (1-\theta) \left( 1 - 1.004\theta + 0.418\theta^3 + 0.21\theta^4 - 0.169\theta^5 \right) \right]^{-1/2}. \quad (14)$$

Non-linear least squares fitting of Eq. (13), substituted with Eq. (14) to the results (Fig. 9), as well as fitting the more complicated expression for a cylindrical pore [40] led to estimates for  $d_{ECS}$  and  $\lambda_{\theta=0}$  [38]. RD theory fit the tissue data well for both models yielding  $d_{ECS} = 37.7$  nm and  $\lambda_{\theta=0} = 1.72$  for parallel planes and  $d_{ECS} = 63.8$  nm and  $\lambda_{\theta=0} = 1.63$  for cylindrical pore geometry [38]. At this time there is insufficient data to choose between the two models so it can only be said that these results suggest that the width of the ECS is between 38 and 64 nm.

These results challenge the long-held view that the width of the ECS is about 20 nm. The 20 nm estimate was based on electron micrographs, however it is well established that conventional electron microscopy tends to obliterate the ECS (see [38] for a summary of the literature) so the new estimate is not implausible. This finding has importance not only for understanding how large an effective signaling molecule can be in the ECS, but also for the design of drug delivery strategies that may employ antibodies, viral vectors or other large vehicles.

## 7. Other modeling issues: binding, uptake and charge

This brief review has focused on physical impediments to diffusion in the ECS but there are other mechanisms that may determine the ability of a molecule to reach a given destination. Chief among these are the possibilities that a specific molecule may bind to a receptor on a cell membrane or be taken up into a cell. Indeed, all molecular signals must eventually undergo this fate in order to be effective.

This mechanism was represented by the general term  $F_{\text{Loss}}$  in Eq. (3). When the binding or uptake is irreversible and proportional to the concentration, an analytical solution to Eq. (3) often may be found. This is exemplified by the solution for the RTI-TMA method described by Eq. (4). This type of kinetics is also appropriate for molecules that are lost into the blood stream across the blood-brain barrier [41]. In many instances of biological interest, however, the binding or uptake process saturates leading to Michaelis-Menten kinetics and non-linear solutions to the diffusion equation. An example of this is the behavior of the neuromodulator dopamine in certain brain regions [42]. Thus in some situations the transport process may be dominated by binding, uptake or loss rather than diffusion.

Finally, if the binding is reversible and the process is brief compared to the general diffusion process, the effect is simply an increased tortuosity [43]; this is essentially the case with small dead-space microdomains and the reason why it is legitimate to employ the diffusion equation for such problems. Some form of fast reversible binding also may underlie non-specific interactions of charged molecules with the fixed negative charge groups on the extracellular matrix; but this interaction is poorly understood at present.

## 8. Conclusion

Diffusion measurements in living brain tissue have revealed that the ECS is a more complex microenvironment than hitherto thought. The geometry may harbor dead-space microdomains, a matrix within the ECS may impede molecular movement and the transport of large molecules may be dominated by the drag of the cellular membranes that form the boundary of the ECS. For some molecules, other effects such as binding, loss or charge interaction may play a major role. So the ECS has the potential to channel molecular signals or be permissive to some but restrictive to others and this behavior may vary from brain region to region. In order to understand these effects and their

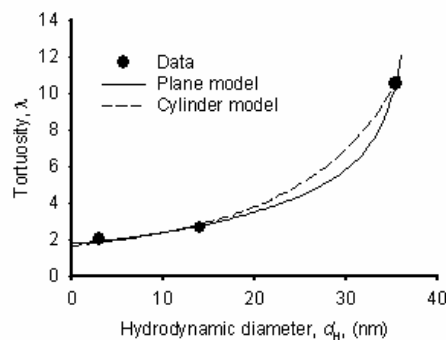


Fig. 9. Fitting of pore models to data. Data points are for measurements in *in vivo* rat cortex with 3 kDa and 70 kDa dextran molecules and with QD655 [38]. Plane model corresponds to model A in Fig. 8, cylinder model to B in Fig. 8.

implications, models are essential and a few have been described here. Other models have been published (e.g. [17, 27, 44, 45]) and modeling the ECS seems a fertile area for physicists and engineers in the future. All modeling, however, needs to be done in concert with careful experiments because Nature never ceases to surprise us!

### **Acknowledgement**

This review is largely based on the careful experimental and theoretical work of my colleagues, Jan Hrabec, Sabina Hrabětová, Lian Tao and Robert G. Thorne. I thank Jyoti Patel for comments on the manuscript. The work was supported by Grant NS-28642 from the US National Institute of Health.

### **References**

- [1] C. Nicholson, Reports on Progress in Physics 64 (2001) 815-884.
- [2] C. Nicholson and E. Syková, Trends in Neurosciences 21 (1998) 207-215.
- [3] S.W. Kuffler and D.D. Potter, Journal of Neurophysiology 27 (1964) 290-320.
- [4] U. Novak and A.H. Kaye, Journal of Clinical Neuroscience 7 (2000) 280-290.
- [5] J.D. Fenstermacher and T. Kaye, Annals New York Academy of Sciences 531 (1988) 29-39.
- [6] C. Nicholson and J.M. Phillips, Journal of Physiology (London) 321 (1981) 225-257.
- [7] C. Nicholson and M.E. Rice. in (Boulton, A.A., Baker, G.B. and Walz, W., editors) Neuromethods: The Neuronal Microenvironment, Humana, Clifton, NJ 1988, pp. 247-361.
- [8] C. Nicholson, Journal of Neuroscience Methods 48 (1993) 199-213.
- [9] M.E. Rice, Y.C. Okada and C. Nicholson, Journal of Neurophysiology 70 (1993) 2035-2044.
- [10] I. Voříšek & E. Syková, Journal of Neurophysiology 78 (1997b) 912-919.
- [11] L. Tao and C. Nicholson, Journal of Theoretical Biology 229 (2004) 59-68.
- [12] J.R. Stiles and T.M. Bartol. in (De Schutter, E., editor) Computational Neuroscience: Realistic Modeling for Experimentalists, CRC Press, London 2001, pp. 87-127.
- [13] J.C. Maxwell, A Treatise on Electricity and Magnetism. Volume 1, 3rd Revised Edition, Dover, New York, 1954, Article 314.
- [14] K.S. Cole, L. Choh-Luh and A.F. Bak, Experimental Neurology 24 (1969) 459-473.
- [15] R.T. Mathias, Biophysical Journal 42 (1983) 55-59.
- [16] A.W. El-Kareh, S.L. Braunstein and T.W. Secomb, Biophysical Journal 64 (1993) 1638-1646.
- [17] J. Hrabec, S. Hrabětová and K. Segeth, Biophysical Journal 87 (2004) 1606-1617.
- [18] R.C. Goodknight, W.A. Klikoff and I. Fatt, Journal of Physical Chemistry 64 (1960) 1162-1168.
- [19] S. Hrabětová, J. Hrabec and C. Nicholson, Journal of Neuroscience 23 (2003) 8351-8359.
- [20] S. Hrabětová and C. Nicholson, Neurochemistry International 45 (2004) 467-477.

- [21] A. Tao, L. Tao and C. Nicholson, *Journal of Theoretical Biology* 234 (2005) 525-536.
- [22] R.A. Siegel and R.L. Langer, *Journal of Colloid and Interface Science* 109 (1986) 426-440.
- [23] K.C. Chen and C. Nicholson, *Proceedings of the National Academy of Sciences of the United States of America* 97 (2000) 8306-8311.
- [24] S. Torquato, *Random Heterogeneous Materials. Microstructure and Macroscopic Properties*. Springer Verlag, New York, 2002.
- [25] A.G. Ogston, B.N. Preston and J.D. Wells, *Proceedings of the Royal Society London A* 333 (1973) 297-316.
- [26] E.M. Johnson, D.A. Berk, R.K. Jain and W.M. Deen, *Biophysical Journal* 70 (1996) 1017-1023.
- [27] D.A. Rusakov and D.M. Kullmann, *Proceedings of the National Academy of Sciences of the United States of America* 95 (1998) 8975-8980.
- [28] L.P. Savtchenko and D.A. Rusakov, *Neuroimage* 25 (2005) 101-111.
- [29] C. Nicholson and L. Tao, *Biophysical Journal* 65 (1993) 2277-2290.
- [30] S. Hrabětová and C. Nicholson. in (Michael, A.C. and Borland, L.M., editors) *Electrochemical Methods for Neuroscience*, CRC Press, Taylor Francis Group, Boca Raton 2007, pp. 167-204.
- [31] S. Prokopová-Kubinová, L. Vargová, L. Tao, K. Ulbrich, V. Subr, E. Syková and C. Nicholson, *Biophysical Journal* 80 (2001) 542-548.
- [32] L. Tao and C. Nicholson, *Journal of Microscopy - Oxford* 178 (1995) 267-271.
- [33] E.L. Cussler, *Diffusion. Mass Transfer in Fluid Systems*. 2nd Edition, Cambridge University Press, Cambridge, 1997, Section 5.2.1.
- [34] S. Hrabětová, *Hippocampus* 15 (2005) 441-450.
- [35] L. Tao and C. Nicholson, *Neuroscience* 75 (1996) 839-847.
- [36] R.G. Thorne, S. Hrabětová and C. Nicholson, *Journal of Neurophysiology* 92 (2004) 3471-3481.
- [37] M. Stroh, W.R. Zipfel, R.M. Williams, W.W. Webb and W.M. Saltzman, *Biophysical Journal* 85 (2003) 581-588.
- [38] R.G. Thorne and C. Nicholson, *Proceeding of the National Academy of Sciences of the United States of America* 103 (2006) 5567-5572.
- [39] W.M. Deen, *AIChE Journal* 33 (1987) 1409-1425.
- [40] P.M. Bungay and H. Brenner, *International Journal of Multiphase Flow* 1 (1973) 25-56.
- [41] C.S. Patlak and J.D. Fenstermacher, *American Journal of Physiology* 229 (1975) 877-884.
- [42] C. Nicholson, *Biophysical Journal* 68 (1995) 1699-1715.
- [43] J. Crank, *The Mathematics of Diffusion*. 2nd Edition, Clarendon Press, Oxford, 1975, Section 14.2.
- [44] L. Dai and R.M. Miura, *SIAM Journal of Applied Mathematics* 59 (1999) 2247-2273.
- [45] R.K. Nandigam and D.M. Kroll, *Biophysical Journal* 92 (2007) 3368-3378.